HELICOPTER ROTOR DOWNWASH CALCULATION USING THE VORTEX ELEMENT METHOD FOR THE WAKE MODELLING

D.G.Papanikas[+++], A.J.Spyropoulos[+], D.K.Fertis[+], D.P.Margaris[++]

[+++]Professor, [++]Lecturer Dr-Eng, [+]Dipl.-Eng., Fluid Mechanics Lab., University of Patras, GR-26500, Patras, Greece

SUMMARY

This paper presents the calculation of the nonuniform induced downwash of a helicopter rotor in forward flight by utilizing an efficient physicomathematical modelling based on the Vortex Element Method (VEM) for the description of the arbitrary vortex wake, which determines the rotor flowfield. The wake model consists of the concentrated tip vortex, the trailing vortices and the shed vorticity which are discretized into vortex elements. The induced velocity is calculated by means of the Biot-Savart law integration over each of these elements. A computer code has been developed for the calculation of the bound circulation distribution, wake geometry and circulation as well as blade airloading. In the computational procedure the rotor wake contraction and distortion, the vorticity dissipation, the vortex core modelling, the inboard vorticity and wake roll up process are numerically simulated and their influences on the rotor downwash are demonstrated.

NOMENCLATURE[*]

$\alpha(r,\psi)$	: local angle of attack distribution
β_0	: the coning angle
φ	: age of a given wake element
ψ	: current blade azimuth
Ω	: rotor rotational speed
c	: rotor blade chord
c_l	: local lift coefficient
c_d	: local drag coefficient
M^*	: critical Mach number
$g_{bv}(r,\psi)$	: bound vorticity circulation distribution
g	: strength of the vortex segments
μ	: advance ratio
R	: rotor blade radius
r_c^*	: critical vortex core radius
r_{cmin}	: minimum vortex core radius
w	: vortex induced velocity
U_T	: local velocity tangential to blade section

[*]only the main symbols are included, all the others are explained in the text.

1. INTRODUCTION

The accurate computation of the induced velocity on helicopter rotor plane is a prerequisite for the precise evaluation of the angle of attack distribution along the rotor blades, which leads to improved airloads prediction for aerodynamics and aeroacoustics design and performance analysis. Early attempts to model the rotor induced downwash, such as the rudimentary uniform inflow approach[1,2] and the Mangler-Squire[3] analytical approach which produces a nonuniform but symmetric induced downwash, are useful only for specific cases. In a more advanced generation the rigid and/or semi-rigid approach for the wake geometry gives usable results when empirical parameters from experiments are applied, s. for example[1,4,5].

On the other end, some complicated models have recently been developed for application with various CFD methods[6]. Their results are in most cases satisfactory but computing time consumption and complexity of the mathematical modelling are increased. Instead, Vortex Element Method (VEM) provides a transparent investigation, concerning the role of various physical parameters which influence the aerodynamic problem of rotor downwash computation.

The concept of free vortex wake with its deformation by the self-induced velocity is fully applied and parameters as wake distortion and geometry, structure and decay of the wake vortices, and blade motion characteristics can be taken into consideration and their influence can be predicted. The sophistication of the physical modelling can be settled to the degree needed in specific applications while the computing time consumption remains relatively small. An extensive overview of recent developments and research activities on this field is given in reference[7].

The discretization of vortical flows in vortex filaments or/and vortex sheet elements is

an established technique originally applied in rotor wake analysis by Brady[8] and Scully[9] whereas recent NASA and academic research has confirmed its application on rotor and propeller flows[10,11]. For this way of analysis the term "vortex element method" is introduced here constituting the most important part of a synthesized methodology for the integrated aerodynamic analysis of helicopter rotors the other being the blade motion and the aerodynamic blade properties. The basic formulation of VEM is closely related to classical vortex methods for boundary layer and vortical flow analysis extensively applied by Chorin[12], Leonard[13] and other researchers (s. the excellent overview of Sarpkaya[14]).

The computational analysis developed combines VEM, which predicts the free wake and the induced flowfield, with a lifting-line and/or lifting-surface based method, for the calculation of the vibratory airloading in several flight conditions. The experimental data used for comparisons include test cases executed during cooperative European research programs on rotorcraft aerodynamics and aeroacoustics performed in the open test section of the German-Dutch Wind Tunnel (DNW) The Netherlands[15]. The resulted integrated computer code, is a very useful tool for the aerodynamic analysis of helicopter rotors.

2. PHYSICOMATHEMATICAL MODELLING

The VEM simulation of the vortical structure of the rotor wake, with discrete straight or curved vortex lines or vortex sheets allows the use of specific models to represent the behavior of the vorticity in an effective free wake calculation scheme. The calculation of the distorted wake geometry provides the induced downwash distribution on rotor disk, which is of primary importance for the rotor vibratory airloading. The computational procedure is based on the assumption that the helicopter rotor performs a steady state equilibrium flight, implying that forward flight speed, rotor rotational speed, tip path plane orientation and wake geometry remain constant with time.

2.1 Vortex wake modelling

On the rotating blades of a helicopter rotor the bound circulation varies both radially and azimuthally. Spanwise circulation variations on rotor blade generate trailing vorticity, g_n, whose direction is parallel to the local flow velocity. On the other hand azimuthal variations produce shed

vorticity radially oriented, g_s, due to the transient nature of the rotor blade flowfield (Fig. 1).

2.1.1 Tip vortex structure

The circulation gradients on rotor blades, determine the strength of the vorticity shed at specific spanwise locations. In general, the bound circulation has a peak near the blade tip while it becomes zero at the tip. This steep gradient creates a high strength trailing vortex sheet which rapidly rolls up and forms the concentrated tip vortex.

The modelling of the tip vortex roll up process is an important aspect in wake aerodynamics and influences the rotor flowfield basically in two ways. First, the roll up model defines the amount of circulation finally concentrated in tip vortex line which in conjunction with the core model used, determines the velocity induced by the tip vortex on rotor disk. Second the modelling of roll up rate, affects the prediction of close Blade Vortex Interactions (BVI) since such phenomena are not expected until the tip vortex line is totally formed.

For the computational procedure developed, the tip vortex strength is determined by a bound circulation model, implying that the circulation of the formed vortex line generated from blade tip at a specific azimuth, $g_t(\psi)$, is equal in magnitude with the bound circulation peak, $g_{bvm}(\psi)$, at that azimuth

$$g_{bvm}(\psi) = g_t(\psi)$$

Since bound circulation distribution changes azimuthally, the tip vortex strength varies along its length, depending on the circulation peak at the moment of vortex line emanation from the blade.

The roll up model included in the computations is based on the assumption that a part of tip vortex circulation is instantaneously concentrated and forms a vortex filament and another part is distributed at a small region behind the rotor blade (about two or three times the chord length, based on experimental observations), before it finally rolls up. By these means, near wake close to blade tip, consists of a vortex sheet plus vortex line (region TV in Fig.1).

After roll up process, the resulting tip vortex line is represented by the straight vortex line segments whose circulation can be constant or linearly varying. Special care has been taken when the curvature of the vortex line becomes important for the computations. This occurs when induced velocity, due to adjacent line segments, is computed at the intermediate ending point. For

these cases the part of vortex line consisting of these straight elements is simulated by curved line segments and the self-induced velocity is computed by appropriate relations.

2.1.2 Vortex core concept and blade vortex interaction (BVI).

The modelling of the viscous core of tip vortex, influences the velocity field induced to rotor disk and alters the calculated airloading. Therefore a model must be derived for the description of the radial vorticity distribution at the region of vortex core. Several models have been developed for the vorticity distribution of real vortices[16,17,9]. In the present analysis, the fixed wing core model has been adopted, which implies a circulation distribution given by:

$$g_c(r_v) = \frac{r_v^2}{1+r_v^2} \qquad (1a)$$

where the circulation $g_c(r_v)$ is normalized by the total circulation of the vortex line and the radial coordinate r_v from the center of vortex line, is normalized by the core radius r_c.

According to experimental observations it can be simplified assumed that:

$$r_c = C_r \frac{c}{R} \qquad \text{with } C_r=0.05 \;^{(9)} \qquad (1b)$$

Especially for tip vortex line segments the rotary wing core model[9] is included as an option. The circulation distribution introduced by this model is:

$$g_c(r_v) = \begin{cases} 0.2r_v^2 / (1+r_v^2) & 0 \le r_v \le 1 \\ 1.0 - 0.9e^{-0.75(r_v-1)} & r_v \ge 1 \end{cases} \qquad (2)$$

The constant C_r of the vortex core radius imposed by this model is 0.008, about an order of magnitude less than fixed wing model.

Special treatment was needed for the magnitude of core radius, r_c, under some physical considerations. The dimensions of the viscous tip vortex core itself influence directly all the phenomena related to interactions of the vortex in the rotor and wake environment.

For small chord lengths and high strength concentrated tip vortices, simplified r_c assumptions have to be used with care. There is a lower limit for the core radius which is dictated by low pressure effects due to high velocities near the vortex axis. For a small core radius these velocities may approach the transonic limit and, at least for frictionless flow, they lead to low densities, breaking down the assumption of a continuum flow. In order to quantify the meaning of the "near" region to vortex axis, the basic dynamic equation can be solved for the vortex flowfield of which the physical streamlines are concentric circles.

In the limiting case of axis proximity the Mach number goes to infinity. Two characteristic vortex core radii can be specified: an absolute minimum core radius r_{cmin} and the critical vortex radius r_c^* defined by the streamline where the circumferential velocity is equal to the speed of sound a_s (at standard conditions $\cong 330$ m/s) or $M^*=1$. According to known relations for isentropic flow inside a potential vortex with circulation g_t the following holds:

$$r_{c\,min} = \frac{g_t}{2\pi a_s}\sqrt{\frac{\gamma-1}{2}}, \quad \frac{r_c^*}{r_{c\,min}} = \sqrt{\frac{\gamma+1}{\gamma-1}} \qquad (3)$$

with $\gamma \cong 1.4$ the isentropic exponent for air.

At time zero, when a free vortex leaves the blade, it can be assumed that the vortex core has at least a finite radius of r_{cmin} according to eq.(3). In a peripheral ring region of $r_c^*-r_{cmin}$ the flow is supersonic, while compressible flow exists in the region $r>r_c^*$ until incompressible Mach numbers are achieved. This hypothetical situation exists only in frictionless flow and the extension of the compressible core regions directly depends on the strength g_t of the vortex at the beginning of its formation. For maximal bound circulation values of 5 to 20 m^2/s of conventional model and full scale rotors respectively, the magnitude of r_{cmin} and r_c^* is of the order of some centimeters (for example for $g_t=10$ m^2/s: $r_{cmin}=2.1$ cm and $r_c^*=5.1$ cm), thus roughly one tenth of a typical rotor blade chord. In any case it seems useful for rotorcraft rotor blades to assume a tip vortex core radius r_c which at the beginning has a value greater than r_{cmin}. This implies that core radius smaller than the above limits are not physically allowed.

Another important aspect of tip vortex aerodynamics related to vortex core modelling is the behavior of the core when close blade vortex encounters occur. The vorticity structure in the core region is influenced during these encounters and the result is the enlargement of the core radius while the circulation of the vortex line is conserved. Various models have been developed to simulate these phenomena and explain the associated effects on airloading. In order to avoid time consuming computation the simplest core bursting model is considered. This model consists

280

of a steep increase of the vortex core radius considering a uniform rate for its propagation along the vortex line. A burst core radius about 10 times the value of r_c was found to be adequate.

The bound circulation distribution is also altered when a concentrated vortex passes in close proximity to a rotor blade. The change of circulation produces an additional shedding of vorticity in the near wake, which in terms affects the induced velocity distribution on the rotor blade in an opposite manner than this of the concentrated vortex. Figures 4 and 5, demonstrate the smoothing of downwash curve as a result of taken into account near wake due to BVI. Comparisons are made with the case of neglecting these near wake effects as well as the vortex core bursting. The figures indicate that neglecting BVI effects, strong variations to both radial and azimuthal distributions appear, which in most cases are unrealistic. In addition, BVI phenomena determine the aeroacoustics of rotor flowfield which makes their exact simulation necessary for noise prediction.

To account for these effects a formula, based on a simplified lifting surface method proposed by Johnson[18], has been adopted. According to this, a correction is made to the velocity induced at a given blade radial station from the rotor wake, due to the interaction of the blade with a vortex passing nearly enough to cause remarkable airloading changes. Therefore an appropriate criterion for the definition of BVI occurrence has to be specified as follows.

A lower limit of BVI influence can be defined as a percentage of blade airloading changes. In this way, any close encounter between a blade and a vortex segment, which causes a loading variation that exhibits the prescribed limit, should be considered as strong BVI. By adjusting this limit, the influence of any interaction between the blade and the wake vortices can be investigated. With these considerations, a parametric study has been done using the computer code, in order to define a reasonable limit which affects the computed airloads significantly. An indicative diagram is shown in figure 6 which presents the control points location on rotor disk, on which the calculated wake induced velocity has been altered over a certain percent (5% for example) due to BVI. As this figure indicates, when this limit is set to a relatively high percent of change, namely 20%, the number of BVI which exceed it is reduced considerably.

Another conclusion derived from this figure is that the presented methodology predicts increased number of BVI at the forward portion of

rotor disk. This is in agreement with the conclusions of other works[9], based on the observation that the tip vortex of one blade, tends to stay closely to rotor disk, till it is forced by the following blade vortex flowfield to move away.

2.1.3 Inboard trailing and shed wake

The inboard trailing wake is generated by the radial variations of the bound circulation inboard the position where the maximum circulation occurs and is shed along this inboard part of the blade. Due to its distributed nature, its precise geometry is not as important as the geometry of the concentrated tip vortex. Thus, the simplified undistorted wake geometry of the skewed helix is adequate for the inboard trailing wake representation. The single vortex-line inboard trailing model is used for the representation of this part of the wake. A large vortex core radius is used in order to avoid any unrealistic blade vortex interactions produced by the model (Fig. 2). The application of this simple model is neither time consuming nor complicated to use, and satisfactory results are obtained for the most cases.

Estimations based on the blade lift distribution show that the circulation of the shed wake is much less, up to an order of magnitude, than the trailing wake circulation. Normally, a vortex-line model is used for the shed wake with the exception of the near shed wake. This model consists of accumulating all the change in bound circulation between adjacent azimuth angles into a shed vortex line extending radially, parallel to the rotor blade. The near shed wake is always modelled by a vortex sheet for a more accurate calculation of its contribution to blade induced flowfield. In any case where vortex sheets are used for the modelling of spatially distributed vorticity, care has been taken for the avoidance of singularities during induced velocity calculations. Especially when near wake regions are modelled by vortex sheets their geometry is accurately specified because even a small error in their location, has an important influence in downwash computations. The edges of vortex sheets, either for inboard or shed wake simulations laying on the blade, are imposed by the bound circulation distribution on the rotor blade, the moment the vorticity was shed.

2.1.4 Wake circulation determination

The strength of the wake vortex elements is determined by circulation conservation from a bound circulation model. For the wake model

described in the previous paragraphs, where both the tip vortex and the inboard trailing wake are modelled by vortex lines, the radial bound circulation model is shown in Fig. 3.

This figure indicates that the shed vortex-line circulation is constant radially according to this model. The variation of $g_s(\varphi)$ depends on $g_{bvm}(\varphi)$, where φ is the age of vortex element:

$$g_s(\phi) = g_{bvm}(\phi) - g_{bvm}(\phi + \Delta\phi) \qquad (4)$$

If the shed vortex-line is used, the trailing-wake circulation will be constant over each vortex-line segment and vary between segments. For the tip vortex-line segment of age φ:

$$g_{t,i} = g_{t,i+1} = g_{bvm}(\phi) \qquad (5)$$

and for the inboard trailing vortex-line segment

$$g_{n,i} = g_{n,i+1} = -g_{bvm}(\phi) \qquad (6)$$

where the subscripts i,i+1 indicate the two ends of a segment, while $g_{bvm}(\varphi)$ is the maximum of bound circulation at age φ.

2.1.5 Vortex wake distortion and geometry

In the present analysis, each vortex element is assumed to be convected with the local velocity of the flowfield, which consists of the rotor forward speed and the velocity component induced by the wake itself. When the bound circulation distribution on the rotor disk is known, the circulation of each vortex element of the wake can be determined with respect to the adopted bound circulation model.

Assuming uniform inflow, the rigid-wake geometry of helical shape is obtained. In terms, a distortion vector $\vec{D}_n$ is determined for every point $P_n(r_w,\varphi)$ in the rotor wake (r_w denotes the polar coordinate of the point), which describes the displacement of point P_n from its initial position (on the rigid wake shape) due to the velocity induced by the wake elements plus the contribution of the bound circulation. When the distortion vector $\vec{D}_n$ is computed for every point P_n the new distorted wake geometry is obtained and the nonuniform induced downwash distribution can be calculated on rotor disk.

Since tip vortex is the dominant part of the rotor wake due to its concentrated structure, its geometry must be accurately specified because it has a great influence on the computed downwash

distribution and airloads prediction. The distributed vorticity, which forms trailing and shed wake, alters the induced velocity on rotor disk but its location can be approximately specified without a significant loss of accuracy.

On the other hand, the distortion calculations can be very time consuming when applied to every vortex element included trailing and shed wake elements. Therefore, for the present work only the distorted tip vortex geometry is computed while trailing wake and shed wake are assumed to have the rigid wake shape.

The aforementioned geometry calculation procedure is adopted for the developed free wake code and has been found to give satisfactory results, in good agreement with other commonly used wake simulations.

A presentation of the computed tip vortex geometry is given in figures 7,8. In these plots, the rotor wake for two different conditions concerning climb and descent flight is shown. Only two tip vortices of a four bladed rotor are plotted with different kind of lines. Both figures are referred to the moment when the corresponding blades are located at azimuth angles $0°$ and $180°$. If the blades were at a different azimuth angle the geometry of the tip vortex would be different because the age of various points P_n on the vortex line would be changed. However, the geometry changes with increasing age are normally slow enough, so that the picture of two tip vortices emanating from two azimuth angles is enough to show the wake behavior. One can notice that for the climb case, a greater part of tip vortices stays near the rotor disk. This is because the advance ratio for this test case (Fig.7) is less than that of the descent case (Fig. 8).

Another approach for the prediction of rotor wake geometry is the "semi rigid" model proposed by Beddoes[5]. The basic assumption is that a uniform inflow is considered, which leads to the rigid-wake geometry, and that the vertical displacement of every vortex element is due to a time averaged induced velocity distribution along the tip path plane. Therefore the tip vortex distorted geometry is calculated from the following relation relative to the nonrotating tip path plane (TPP) axis system, using an appropriate model or experimental data, for the induced velocity distribution on the rotor disk $w(r,\varphi)$:

$$\vec{r} = \left(R\cos(\psi - \phi) + \mu\phi\right)\vec{i} + R\sin(\psi - \phi)\vec{j} +$$
$$+ \left(R\beta_0 + \frac{w\sin\alpha_D}{\Omega R}\phi + \frac{1}{\Omega R}\int_0^\phi w(r,\phi)d\phi\right)\vec{k} \qquad (7)$$

where R is the blade radius, Ω the rotor rotational speed, φ the age of the given wake element, ψ the current blade azimuth, μ the advance ratio and β_0 the coning angle.

In this way the model provides a semi-analytical solution of rotor wake geometry implying that a function of induced velocity distribution on rotor TPP is given. Calculations based on this model for several cases have shown that it can be applied only for preliminary studies on rotor wake geometry predictions. Since free wake approach provides a better simulation because interaction between wake elements during wake evolution is accounted, the present work is based on this approach.

2.1.6 Vorticity dissipation in the wake

The effect of viscosity on real vortices is to diffuse the vorticity and to create a vortex core which increases its diameter until there is a balance by the inward velocity component. The decaying nature of a viscous vortex can be represented by the following relation:

$$ w = \frac{g_0}{2\pi r} \cdot \left(1 - \exp\left(-\frac{r^2}{4 \cdot v \cdot t} \right) \right) \tag{8} $$

where w is the vortex induced velocity, g_0 the total circulation of the vortex , r the radial distance from the vortex segment, t the time, and v the kinematic viscosity coefficient. Eq.(8) is a solution of the Navier-Stokes equation for the laminar vortex due to Oseen, but the Taylor solution can also be applied. This described nature of real vortices can be adopted to the modelling of the 3-D vortex wake of the rotor, since it influences significantly the calculated induced velocities.

2.2 Induced velocity calculation

Only for the simplest of rotor wake geometry, where the self induced distortion of the wake is neglected, it is possible to calculate the Biot-Savart law integral, performing a direct numerical integration over the whole wake[4]. Even in these cases the solution is not efficient as it requires a very small step in order to obtain accurate results.

Vortex element method overcomes these problems by discretizing the wake into a multitude of vortex elements where the Biot-Savart law can be analytically integrated. The contribution of a finite length vortex line element at an arbitrary point j in the flowfield is obtained by application of the Biot-Savart law:

$$ \vec{w}_{ij} = -\frac{1}{4\pi} \int \frac{g_i \left(\vec{r}_{ijm} - s \cdot \vec{e}_s \right) x d\vec{s}}{\left| \vec{r}_{ijm} - s \cdot \vec{e}_s \right|^3} \tag{9} $$

where $\vec{r}_{ijm}$ is the minimum distance from the vortex line i to the point j, $\vec{e}_s$ the unit vector in the direction of the vortex segment, g_i the strength of the vortex segment i and s the coordinate measured along the vortex segment. In order to overcome the singularity which occurs when self induced velocity is computed from the above expression, the vortex core concept introduced in paragraph 2.1.2 is used.

The velocity induced to a point j from a finite straight vortex line segment i, of constant circulation g_i, with arbitrary orientation, can be derived from eq.(9) considering the vortex core effect and the relative geometrical distances:

$$ \vec{w}_{ij} = \frac{g_i}{4\pi} \, \vec{r}_{i1,j} \times \vec{r}_{i2,j} \, \frac{N}{D} \tag{10} $$

$$ N = \left(\left| \vec{r}_{i1,j} \right| + \left| \vec{r}_{i2,j} \right| \right) \left[1 - \left(\vec{r}_{i1,j} \, \vec{r}_{i2,j} \right) / \left(\left| \vec{r}_{i1,j} \right| \, \left| \vec{r}_{i2,j} \right| \right) \right] \tag{11} $$

$$ D = \left| \vec{r}_{i1,j} \right|^2 \left| \vec{r}_{i2,j} \right|^2 + \left(\vec{r}_{i1,j} \, \vec{r}_{i2,j} \right)^2 + $$
$$ + r_c^2 \left(\left| \vec{r}_{i1,j} \right|^2 + \left| \vec{r}_{i2,j} \right|^2 - 2 \, \vec{r}_{i1,j} \, \vec{r}_{i2,j} \right) \tag{12} $$

Another important effect on downwash calculations is due to the close blade interactions (BVI) mentioned in paragraph 2.1.2.

Induced downwash as well as blade airloading, is calculated on specific radial stations on each rotor blade for an azimuthal step $\Delta\psi$. The number and distribution of these radial stations must be chosen with care. Poor discretization may lead to inaccurate results, because important BVI phenomena may be missed, while too fine discretization increases computing time. A more dense distribution should be applied at blade tip, since it is an area of rapid variations, while fewer radial stations can be used towards the blade root.

Several trial runs have been made using the developed computer code in order to determine a reliable number of radial stations which is a trend between accuracy and computing consumption. Indicative diagrams are presented here in figures 9, 10 for comparisons between 6 and 12 radial control points, concerning downwash computations.

From these diagrams can be concluded that radial distributions of downwash are affected mostly from the finer spanwise discretization. Especially control points which lay between the primary 6 stations seem to "capture" some

downwash variations which otherwise would be lost. Such a fact has a significant influence on airloads computations also. On the other hand, at some spanwise locations where the two discretizations coincide the results are similar. At blade tip where the two distributions are more dense there are no considerable differences to computations. A bigger number of radial control points does not seem to cause any further improvement.

2.3 Airloads calculation

The accurate calculation of rotor downwash distribution, is the basis for realistic predictions of rotor harmonic airloads. Nonuniform wake induced flowfield is the primary reason for the vibratory character of rotor blade airloading.

Since VEM provides a good simulation of the distorted wake geometry, the induced inflow on rotor disk is calculated by integration of the Biot-Savart law in closed form. Modifications of the original inviscid flow relations are made, concerning viscous core modelling. When downwash distribution has been calculated, the blade section angle of attack distribution is obtained from the relation:

$$\alpha(r, \psi) = \theta(r) - \tan^{-1}(U_P / U_T) \tag{13}$$

where U_P is the air velocity perpendicular to No Feathering Plane (NFP), and U_T is the tangential velocity to blade airfoil at a radial station, both normalized by tip speed ΩR, and $\theta(r)$ is the collective pitch angle.

Rotor blades fulfill the request for high aspect ratio wings and therefore the lifting line solution for the blade section lift calculation is applicable for the most cases. Following this method, the bound circulation is calculated by the an expression based on Kutta-Joukowski condition:

$$g_{bv}(r, \psi) = 0.5 \, U_T(r, \psi) \, c(r) \, c_l(\alpha, M, Re) \tag{14}$$

In the above expression c is the section chord, c_l is the lift coefficient, and α is the angle of attack distribution given by eq.(13). The circulation $g_{bv}(r, \psi)$ is normalized by the factor $(\pi c \Omega R)$. Angle of attack, Reynolds and Mach numbers are local values at every point (r, ψ).

Since lifting surface effects due to BVI alter the induced downwash on the rotor blade and therefore the local angle of attack, the airloads are expected to be influenced as the same. To justify this, figure 11 is given, which

shows an azimuthal airloads distribution computed with and without lifting surface method. Thus, when lifting surface is included, smaller airload peaks are predicted. This follows the conclusion derived for downwash distribution at paragraph 2.1.2. Also a plot of airloads isocontours is provided in figure 12 which shows that bigger airloads peaks are computed near blade tip.

With known downwash distribution, a blade motion computation is performed. Rotor blade dynamic behavior is important for helicopter rotor downwash computations, to the extent that it influences the angle of attack distribution seen by the blade, and therefore alters bound circulation distribution.

In the developed procedure a simplified blade motion solution has been adopted which considers all harmonics of rigid body flapping and first mode of flapwise bending. A new angle of attack distribution is computed, including blade motion influences, and the blade section lift and drag forces are derived by the expression:

$$F(r, \psi) = 0.5 \, \rho \, c(r) \, U_T^2(r, \psi) \, K(r, \psi) \tag{15}$$

In the above expression $F(r, \psi)$ can be either section lift $L(r, \psi)$ or section drag force $D(r, \psi)$, while $K(r, \psi)$ express lift or drag coefficient respectively. Both coefficients can be directly taken from tables or diagrams in polynomial form. An alternative simplified way is to extract c_l and c_d from the lift curve slope according to the relations:

$$c_l(r, \psi) = \partial c_l / \partial \alpha \; \alpha(r, \psi) = c_{ls} \, \alpha$$
$$c_d = f(c_l) \tag{16}$$

The slope c_{ls} is depending upon the contour of the airfoil section used and is influenced by the local Mach and Reynolds number. The unsteadiness of the rotor blade flowfield also affects the lift curve significantly. For specific airfoil sections, simplified formulas for computing c_{ls} can be derived from corresponding experimental data, according to a methodology mentioned by Prouty[19].

3. COMPUTATIONAL PROCEDURE

The nonuniform helicopter rotor downwash calculation consists of two individual modules. One module performs the free wake calculations based on VEM and provides as output the distortion vector $[\vec{D}]$ which gives the position of every wake vortex element. The other module computes the wake induced downwash on the rotor disk and the resulting airloading. These two

modules as well as the blade motion module are linked in an integrated computational system and are coupled with a matching procedure. This structure provides a great flexibility in accumulating data of any measured or calculated distorted wake geometry. In this way a useful insight on the factors which have important effects on rotor downwash distribution is provided.

3.1 Free wake computations

The free wake computation needs an initial assumption of rotor wake geometry. This assumption can be either the rigid wake geometry or any other which is provided as an input. After the first estimation, an iterative calculation begins and the new position of each vortex element is defined, taking in account the contribution of all the wake elements. A new iteration starts with an assumed wake consisting of the distorted wake from the previous iteration. The iteration scheme continues until distortion convergence is achieved.

The free wake analysis provides a more realistic downwash distribution on rotor disk than rigid wake assumption. In figure 13, the effects of the computed free wake geometry on azimuthal downwash distribution at blade tip are compared with the rigid wake case. As shown for the test case considered, though the curve shape is similar, significant changes can occur at some azimuths which can lead to different airloads predictions.

3.2 Downwash computations

The resulted, after iteration convergence, distorted wake geometry, remains constant during induced velocity calculations. Therefore, the contribution of each vortex element to the rotor flowfield depends on its strength and its orientation relative to rotor disk.

The bound circulation model adopted and vorticity conservation requires constant bound circulation equal to the radial maximum, from the point where the inboard trailing vortex originates to the tip of the blade. The above described model for the wake and bound vorticity representation is shown in Fig. 3. Using this model, the bound circulation calculation problem is reduced to the evaluation of the vector $[g_{bvm}]$ which consists of the radial maximum of bound circulation for each azimuth. Considering the set of vortex segments which constitutes the trailing wake behind a rotor blade, we can calculate the induced velocity at the point i using the relation:

$$w_{nij} = \sum_j g_{nj} f_{nij} \qquad (17)$$

where w_{nij} is the induced velocity contribution from the trailing wake element j at the control point i, g_{nj} the circulation of the segment and f_{nij} the influence coefficient of the segment j to the control point i, which depends only on segment's location. In order to obtain the induced velocities at the N_c control points on rotor disk, and since the g_{nj} values correspond directly to the elements of the vector $[g_{bvm}]$, we can write in matrix form:

$$[F_n] \cdot [g_{bvm}] = [W_n] \qquad (18)$$

Considering the shed wake, the velocity induced from the shed vortex segments at the control point i is obtained using the relation:

$$w_{sij} = \sum_j \left(g_{s(\phi)} - g_{s(\phi+\Delta\phi)} \right)_j f_{sij} = \sum_j \Delta g_{sj} f_{sij} \qquad (19)$$

where the term Δg_{sj} is the circulation of the segment j and the values $g_{s(\phi)}$ and $g_{s(\phi+\Delta\phi)}$ correspond to two successive elements of the vector $[g_{bvm}]$. The velocities induced at the N_c control points from the shed wake are calculated using the following matrix equation:

$$[F_S] \cdot [A] \cdot [g_{bvm}] = [W_S] \qquad (20)$$

where [A] is a correlation matrix between vectors $[\Delta g_s]$ and $[g_{bvm}]$. Hence, the total velocity induced by the trailing and shed wake at the control points of the rotor can be evaluated as a function of the vector $[g_{bvm}]$ by utilizing the aforementioned matrix equations.

With given wake geometry the influence matrices are computed, which depend only on the wake geometry and the position of the blades, and remain constant during the bound circulation iteration. The initial bound circulation distribution $g_{bv0}(r,\psi)$ is obtained from a blade element solution under the uniform inflow assumption. Then, the unknown vector $[g_{bvm}]_0$ is assembled from the initial distribution and is used to compute the induced velocities at the control points for each azimuth. The next step is to calculate the blade motion and the angle of attack distribution $a_1(r,\psi)$. This calculation is followed by the bound circulation distribution calculation given by eq.(14).

Using the above distribution the solution vector $[g_{bvm}]_1$ is computed, by applying the basic wake model, as the radial peak of the $g_{bv}(r,\psi)$ distribution. The procedure is continued with the recalculation of the induced velocities using the

new vector $[g_{bvm}]_1$, the blade motion calculation and the angle of attack distribution $\alpha(r,\psi)$. A new iteration step starts by computing the distribution of the bound circulation $g_{bv(i+1)}(r,\psi)$ as a weighted average of the distribution obtained from the new angle of attack $\alpha(r,\psi)$ and the old value of the circulation distribution:

$$g_{bv(i+1)}(r,\psi) = R_w g_{bv(i+1)}(r,\psi) + \\ +(1-R_w) \cdot g_{bv(i)}(r,\psi) \tag{21}$$

In the above expression R_w is an adjustable weight factor with a typical value of 0.5. The procedure is continued by recalculation of the vector $[g_{bvm}]$, downwash calculation etc., until convergence is achieved for the $[g_{bvm}]$ values. An adequate test for convergence is the comparison of two successive values of the unknown vector $[g_{bvm}]$. The converged downwash distribution is used for the airloads calculations. A plot of downwash distribution isocontours on rotor disk is given in figure 14.

4. CONCLUDING REMARKS

The primary objective of this paper has been to describe the implementation of a computational procedure for helicopter rotor downwash calculations, which utilizes the Vortex Element Method for free wake modelling.

The formulation of rotor wake discretization and the resulting induced downwash predictions were analyzed. The major features of the rotor blade lifting line/lifting surface aerodynamic model have been outlined. Several aspects of rotor wake simulation, such as tip vortex roll up process and vortex core modelling included in the presented methodology were discussed in some detail.

An integrated computer code has been developed applying the presented procedure. Since is based on a flexible coupling between different modules, it becomes a useful tool for the aerodynamic study and optimization of helicopter rotors.

Several cases concerning a variety of rotor flight conditions were tested and indicative diagrams have been presented, demonstrating the benefits of using the vortex element approach for the free wake simulation. Blade vortex interaction effects on downwash computations, the influence of radial control points number and distribution on predicted airloads, lifting line/lifting surface applicability on blade modelling are some of the basic topics discussed in this paper. Most of the results presented concern a full scale H34 rotor,

whose aerodynamic field and behavior has been thoroughly analyzed and measured. The developed computer code has also been tested by comparisons with measurements performed in DNW facility, in the framework of HELINOISE European project. The results were found to be encouraging as can be seen in figures 15, 16 presenting radial and azimuthal lift coefficient distributions.

The presented computational methodology is under further development regarding more sophisticated models for blade aerodynamic and dynamic characteristics as well as optimization techniques for wake geometry calculations.

5. REFERENCES

1. Stepniewski, W.Z., Keys N., "Rotary wing aerodynamics", Dover, N.Y. 1984.
2. Johnson, W., "Helicopter theory", Dover, 1994.
3. Mangler, K.W., and Squire, H.B., "The induced velocity field of a rotor", R&M 2642, 1950.
4. Baskin, V.Y., Vildgrude, L.S., Vozhdayey, Y.S., and Maykapar, G.I., "Theory of lifting airscrews", NASA TTF-823, Feb. 1976.
5. Beddoes, T.S., "A wake model for high resolution airloads", U.S. Army / AHS Int. conf. Rotorcraft Basic Research, Feb. 1985.
6. Bagai, A., and Leisman, G.I., "Rotor free-wake modelling using a pseudo-implicit technique including comparisons with experimental data", Journal of American Helicopter Society, Vol. 40, No. 3, July 1995.
7. "Aerodynamics of rotorcraft", Course held at von Karman Institute in Brussels, AGARD R-781, April 1990.
8. Brady, W.G., and Crimi, P., "Representation of propeller wakes by systems of finite core vortices", CAL Rep. No. BB-1665-5-2 Cornell Aeron. Lab., Cornell University, Buffalo N.Y., February 1965.
9. Scully, M.P., "Computation of helicopter rotor wake geometry and its influence on rotor harmonic airloads", M.I.T., ASRL TR 178-1, March 1975.
10. Bliss, D.B., Teske, M.E., and Quackenbush, T.R., "A new methodology for free wake analysis using curved vortex elements", NASA CR-3958, 1987.
11. Quackenbush, T.R., Wachspress, D.A., and Boschitsch, A.H., "Rotor aerodynamic loads computation using a constant vorticity contour free wake model", AIAA Journal of Aircraft, Vol. 32, No. 5, Sep.-Oct. 1995.
12. Chorin, A.J., "Computational Fluid Mechanics", Academic Press, 1989.

13. Leonard, T., "Computing three dimensional incompressible flows with vortex elements", Ann. Rev. Fluid Mech., Vol. 17, pp. 523-559.

14. Sarpkaya, T., "Computational methods with vortices - The 1988 Freeman scholar lecture", ASME Journal of Fluids Engineering, Vol. 111, No. 5, March 1989.

15. Splettstoesser, W.R., Niesl, G., Cenedese, F., Nitti, F., and Papanikas, D.G., "Experimental Results of the European HELINOISE Aeroacoustic Rotor Test", JAHS, Vol. 40, No. 2, April 1995.

16. Betz, A., "Verhalten von Wirbelsystemen", Zeitschr. Angew. Math. Mech. (ZAMM), Bd.12 (1932), 164-174. (Also NACA TM-713, June 1933)

17. Windnall, S.E., and Wolf, T.L., "Effect of tip vortex structure on helicopter noise due to blade vortex interactions", AIAA Jour. of Aircraft, Vol. 17, No. 10, Oct. 1980, pp. 705-711.

18. Johnson, W., "A comprehensive analytical model of rotorcraft aerodynamics and dynamics", NASA TM-81182, June 1980

19. Prouty, R.W., " Helicopter Performance, Stability, and Control", R. E. Krieger Publ., 1990.

ACKNOWLEDGMENTS
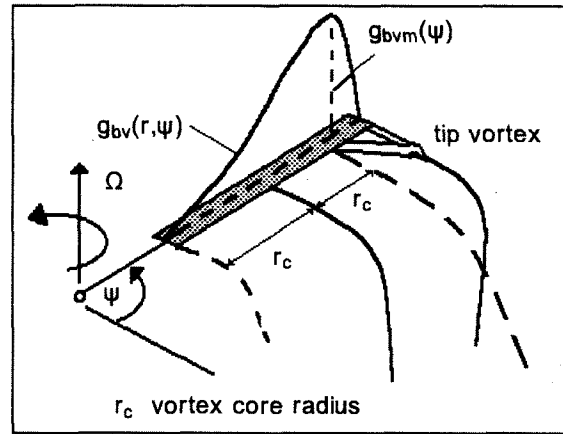
Fig.2 Vortex line modelling for the representation of the inboard trailing wake by a single vortex with core radius r_c.
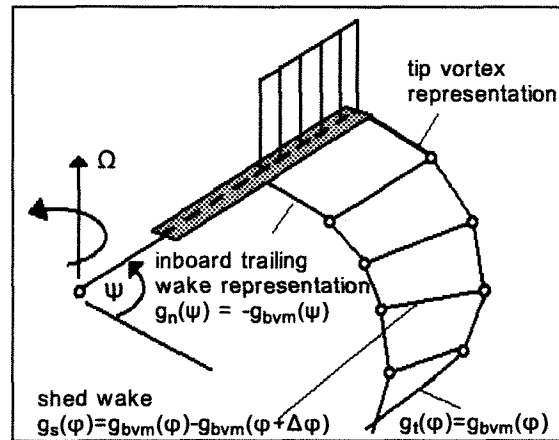
Fig.3 Bound circulation model and wake representation using vortex line segments
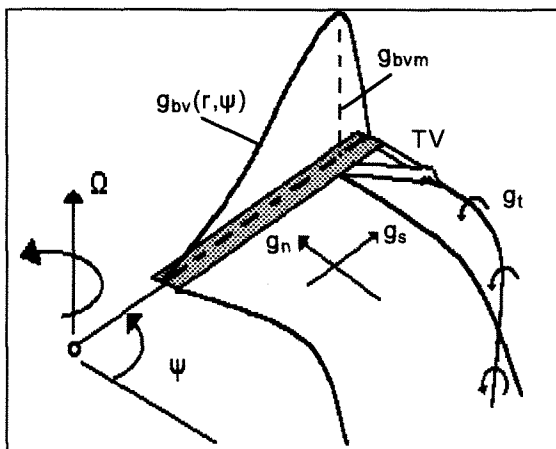
Fig.1 Representation of the tip vortex and inboard trailing vorticity of a rotor blade.
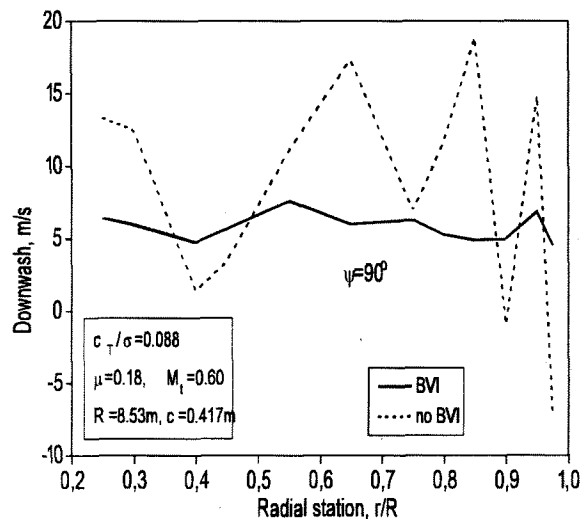
Fig.4 Computed spanwise downwash distribution indicating BVI effects on wake induced flowfield.

287
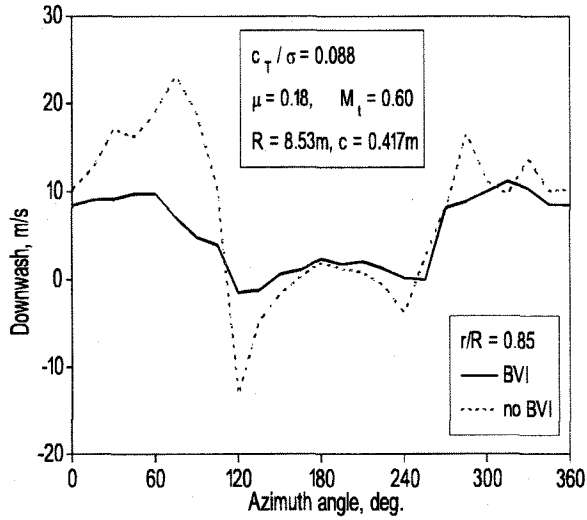
Fig.5 Azimuthal downwash distribution indicating BVI effects. Smaller
peaks are computed when BVI influence on induced velocity is included.
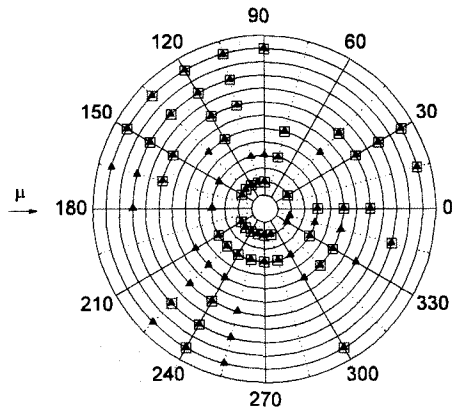
Fig.6 Radial stations (regarded test case c_T / σ = 0.088,
μ =0.18, M_t =0.60, R =8.53m, c =0.417m), on which the
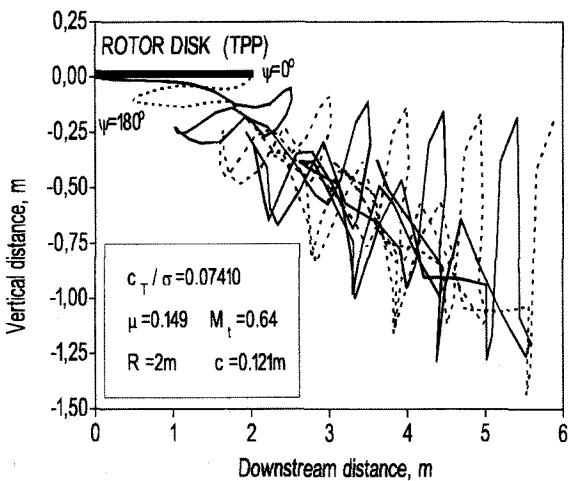induced velocity computed has been altered due to blade
vortex interactions over: 20% □ ,5% ▲

Fig. 7 Free wake geometry calculated for an experimental test case with
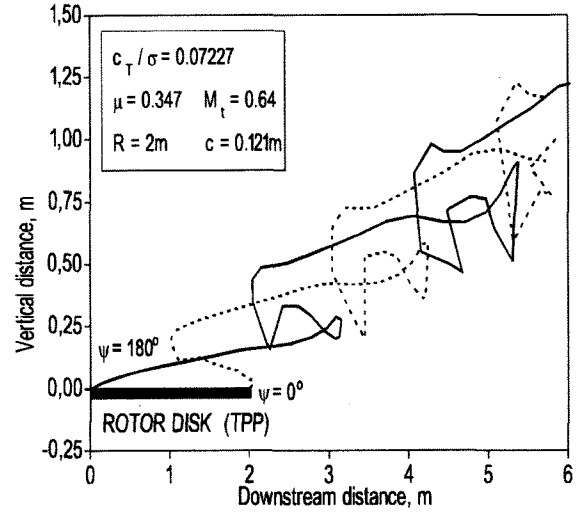climb flight conditions. Only two tip-vortices are shown for simplicity.

Fig. 8 Free wake geometry calculated for an experimental test case with
descent flight conditions. Only two tip-vortices are shown for simplicity.
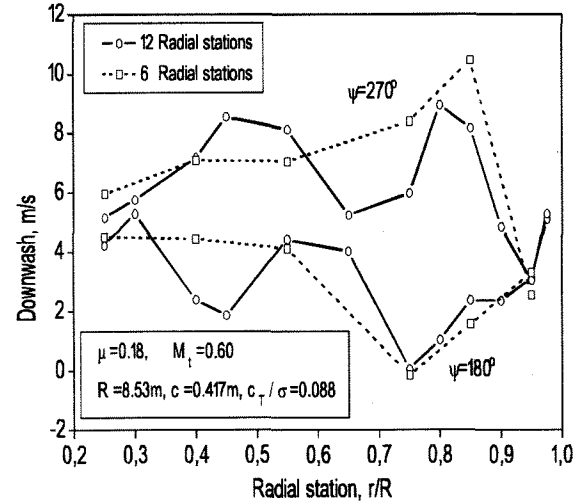
Fig.9 Spanwise downwash distribution at two different azimuthal
angles calculated with 6 and 12 spanwise control stations
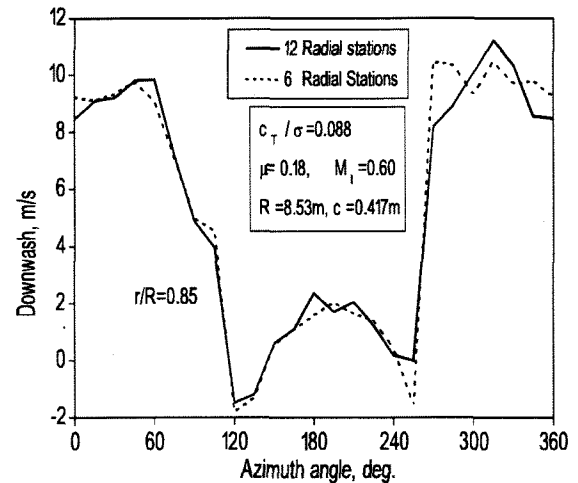
Fig. 10 Downwash azimuthal distribution at 0.85 radial station
calculated using 6 and 12 radial control points.

288
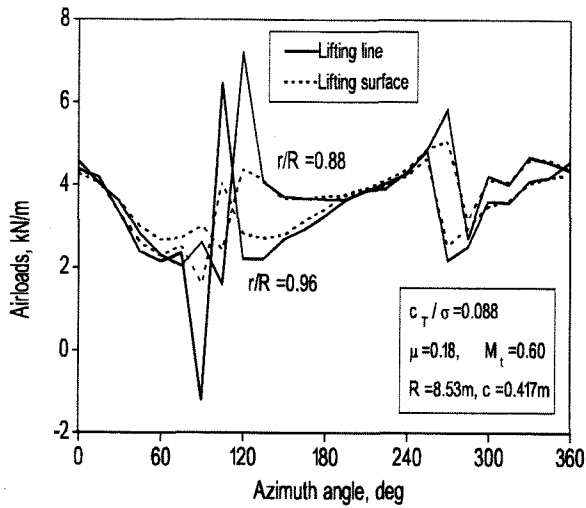
Fig. 11 Azimuthal distribution of blade airloading computed with Lifting Line and Lifting Surface method indicating differences at specific azimuths.
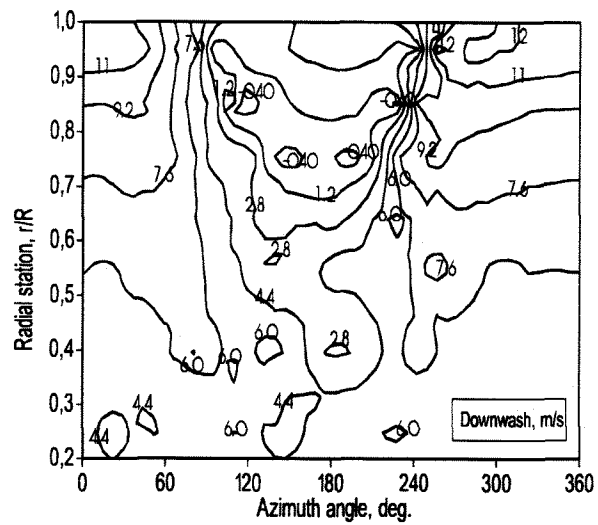

Fig. 14 Free wake downwash distribution on rotor disk. Regarded test case: $c_T / \sigma = 0.008$, $\mu = 0.18$, $M_t = 0.6$, $R = 8.53$m.
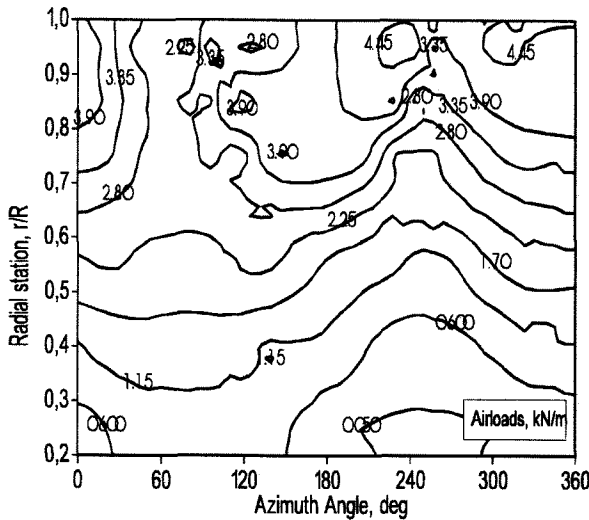

Fig. 12. Rotor disc airloads distribution computation, regarded test case $c_T / \sigma = 0.088$, $\mu = 0.18$, $M_t = 0.60$, $R = 8.53$m, $c = 0.417$m
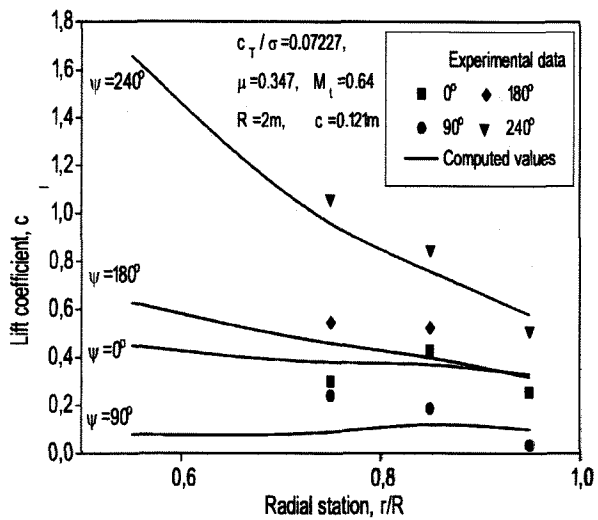

Fig.15 Comparison of blade section lift coefficient between computed values and experimental data regarding a descent test case.
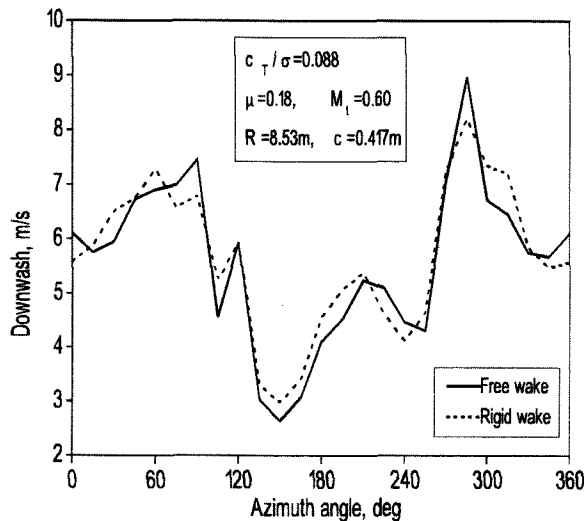

Fig. 13 Downwash distribution calculated at station r/R=0.95.
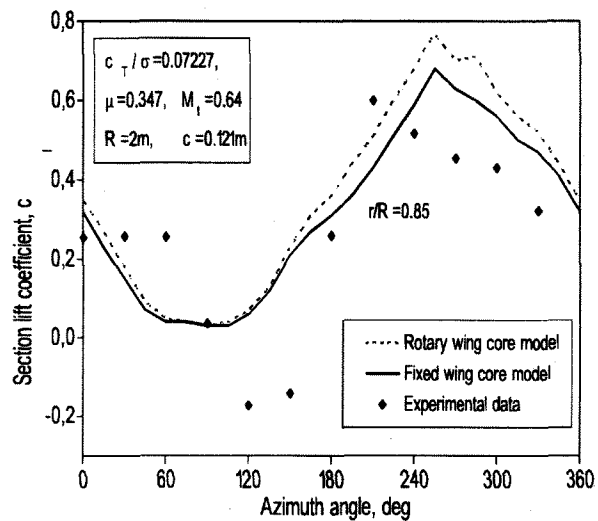Comparison between free wake and rigid wake assumption.

Fig. 16 Section lift coefficient computations comparing fixed and rotary wing core model with experimental data.